ECOHYDROLOGY
Ecohydrol. **6**, 24–37 (2013)
Published online 12 March 2012 in Wiley Online Library
(wileyonlinelibrary.com) DOI: 10.1002/eco.1263

Ecogeomorphic expressions of an aspect-controlled semiarid basin: II. Topographic and vegetation controls on solar irradiance

Hugo A. Gutiérrez-Jurado[1] and Enrique R. Vivoni[2]*

[1] *Department of Earth and Environmental Science, New Mexico Institute of Mining and Technology, Socorro, NM 87801, USA*
[2] *School of Earth and Space Exploration and School of Sustainable Engineering and the Built Environment, Arizona State University, Tempe, AZ 85287, USA*

ABSTRACT

Topography-mediated microclimates give rise to opposing hillslope ecosystems in north facing and south facing slopes of a semiarid basin in central New Mexico. It is hypothesized that large solar irradiance differences are a driving mechanism in the observed vegetation patterns. Using a distributed solar radiation model, we explore the topography–vegetation controls on annual and seasonal irradiance in the basin. Three digital elevation models (DEMs), ranging from 1 m to 10 m resolution, and a digital surface model with tree canopies, from Light Detection and Ranging (LiDAR), are used to assess improvements in capturing irradiance differences in the opposing slopes. Remarkably reduced irradiance is found in the north facing slope throughout the year. This suggests that terrain aspect is a first-order control on the spatial distribution of irradiance, with terrain slope leading to differences within each aspect. Tree cover and its spatial arrangement are important second-order controls on irradiance which can overwhelm topographic effects in specific locations and times of year. For example, differences between north facing and south facing slopes are maximized in the spring equinox, rather than the winter solstice, when tree shading and reflection are accounted for. North facing trees also diminish intercanopy radiation, depending on tree cover and vegetation albedo, with important ecological implications for the conifer–grass association. Solar irradiance analysis helps identify the underlying topographic and vegetation controls on microclimate in the opposing hillslope ecosystems, suggesting a feedback mechanism that helps reinforce the differences in vegetation establishment. Copyright © 2012 John Wiley & Sons, Ltd.

KEY WORDS solar radiation; terrain analyses; albedo; LiDAR; vegetation patterns; ecohydrology

INTRODUCTION

Understanding the effects of terrain attributes on ecologic and hydrologic properties of semiarid areas is highly relevant for a wide range of disciplines (e.g. Holland and Steyn, 1975; Kirkpatrick and Nunez, 1980; Guisan and Zimmermann, 2000; Coblentz and Riitters, 2004; Bennie *et al*., 2008a,2008b; Burnett *et al*., 2008; Ivanov *et al*., 2008a,2008b; Rinehart *et al*., 2008). In mid-latitude regions, semiarid landscapes are sensitive to the controls imposed by topography on the distribution of light, water and nutrients (Holland and Steyn, 1975; Holland *et al*., 1977; Badano *et al*., 2005; Caylor *et al*., 2005). In these water-limited environments, the relative abundance of vegetation is dictated by terrain-mediated energy inputs, the redistribution of available resources and by the ecophysiological adaptations of the plants themselves (Meentemeyer *et al*., 2001; Walton *et al*., 2005). Holland and Steyn (1975) provided a first attempt to address the effects of topographic and latitudinal variations of solar irradiance on vegetation occurrence and response. A number of studies have also recognized the influence of slope and aspect on the modification of the energy budget for mid-latitude ecosystems and its effect on soil moisture availability for plants (Ranzi and Rosso, 1995; Breshears *et al*., 1998; Zou *et al*., 2007).

Systematic variations in the water and energy budgets at different terrain locations can promote the establishment of diverse plant functional types (e.g. grasses, shrubs, trees). Strong variations in ecosystem properties can, in turn, directly impact hydrologic processes, such as interception, infiltration and evapotranspiration, which may promote a self-reinforcing effect on the differential plant establishment (e.g. Nieve and Abrahams, 2002; Wilcox *et al*., 2003; Gutiérrez-Jurado *et al*., 2007). As a result, terrain controls on irradiance may lead to the development of niches in semiarid landscapes that enhance ecosystem diversity as a function of aspect and slope (Kirkpatrick and Nunez, 1980; Horsch, 2003; Walton *et al*., 2005). Contrasting ecosystem properties in topographically complex semiarid basins can also promote differences in hydrogeomorphic processes, as discussed in Part I of this work (Gutiérrez-Jurado and Vivoni, 2012). In Part II, we analyse the topographic and vegetation effects on solar irradiance by using four elevation datasets. We explore the effects of aspect, slope and vegetation on the annual and seasonal radiation, with an emphasis on differences between north facing and south facing regions and the impact of tree shading in

*Correspondence to: Enrique R. Vivoni, School of Earth and Space Exploration, Bateman Physical Sciences Center, F-Wing, 650-A, Arizona State University, Tempe, AZ, USA. E-mail: vivoni@asu.edu

Copyright © 2012 John Wiley & Sons, Ltd.

intercanopy areas. Our intent is to help elucidate the controls on the microclimate in the opposing hillslope ecosystems.

Vegetation–topography–radiation interactions

The effects of topography and vegetation properties on the incident irradiance have been addressed primarily at the hillslope scale (e.g. Breshears *et al*., 1998; Martens *et al*., 2000; Zou *et al*., 2007). Notably, Zou *et al*. (2007), in a systematic study of topography–vegetation cover interactions, demonstrated the effect of plant canopies in reducing near ground solar irradiance for north facing and south facing slopes. Nevertheless, their analysis was performed using precise north facing and south facing aspects and did not account for variations in the aspect or slope occurring naturally in a landscape. From an ecogeomorphic perspective, it is important to study the coupled effects of vegetation and topography on solar irradiance in a complex setting that provides a range of potential vegetation niches (Wilkinson and Humphreys, 2006). Natural landscapes obtained from digital elevation models (DEMs) provide the opportunity to address vegetation–topography interactions when other factors (e.g. geological substrates) can be isolated (Yetemen *et al*., 2010). Investigating the controls of vegetation and topography on irradiance represents a first step in unravelling the complex interactions that lead to aspect-controlled ecosystems in semiarid basins and their effects on landscape morphology (Paola *et al*., 2006).

Vegetation–topography–radiation interactions are considered to lead to the development of microclimates by imposing spatial heterogeneities in energy loads at canopy and intercanopy locations (Breshears *et al*., 1997). As discussed in Gutiérrez-Jurado and Vivoni (2012), terrain features (slope, aspect, curvature) and vegetation obstructions can lead to strong variations in the amount of irradiance reaching the surface. Topographic and vegetation controls may amplify the differences in the microclimate, leading to a wide range of site conditions in a relatively small area (Kirkpatrick and Nunez, 1980). For example, substantial differences in solar radiation within short distances can promote soil thermal gradients that produce varying evapotranspiration rates and affect the soil moisture status (Breshears *et al*., 1997, 1998). These topographically mediated differences can also be amplified or muted by the presence of vegetation itself, through its role on radiation absorption (shading) and reflection (albedo) on a sloping terrain surface. As a result, vegetation–topography–radiation interactions in semiarid basins may reinforce the microclimate conditions that originally led to the vegetation patterns.

Impact of terrain resolution on simulated irradiance

The spatial resolution of the DEM used to analyse the vegetation–topography–radiation interactions directly affects the definition of surface landforms and terrain properties (e.g. Zhang and Montgomery, 1994; Deng *et al*., 2007). For instance, high-resolution DEMs (1 m) increase the range of slope and aspect values, as compared to coarser products (Kienzle, 2004; Gutiérrez-Jurado and Vivoni, 2012). Terrain parameters (slope, aspect and sky view) interact directly with calculations of solar irradiance because the size, shape and orientation of obstructions modify the exposure to solar beam (Suri and Hofierka, 2004). Prior studies have typically used coarse resolution DEMs (~25 to 100 m) (Rich *et al*., 1995; McKenney *et al*., 1999; Dymond and Johnson, 2002; Fu and Rich, 2002; Zaksek *et al*., 2005; Piedallu and Gégout, 2008), though Burnett *et al*. (2008) obtained insolation estimates with a 3 m DEM. Radiation estimates with coarse DEMs have been used to obtain proxies for vegetation productivity and evapotranspiration, among other ecological variables (e.g. Horsch, 2003; Lassueur *et al*., 2006; Astrom *et al*., 2007; Bennie *et al*., 2008a). However, an increasing number of technologies provide high-resolution DEMs (Slatton *et al*., 2007; Tarolli *et al*., 2009) which can be used to study radiation variability at fine resolutions. To our knowledge, however, there are no prior studies addressing the effect of spatial resolution on solar irradiance modelling in areas of complex terrain. Montero *et al*. (2009) used adaptive triangular meshes for improved solar radiation modelling but did not address the resolution issue. Assessing the impact of spatial resolution on irradiance can help determine the level of detail required to capture microclimatic variations that lead to ecogeomorphic differences.

SOLAR RADIATION MODELLING AND OBSERVATIONS

Topographic effects on solar radiation of the ~0.1 km^2 study basin within the Sevilleta National Wildlife Refuge, New Mexico, were studied using the three DEMs introduced in Part I: IFSAR (10 m), dGPS (4 m) and the bare earth LiDAR (1 m). In addition, a digital surface model extracted from the LiDAR data was used to capture the effects of conifer trees (one-seed junipers, *Juniperus monosperma*) on the north facing slope (referred to as 'vegetated LiDAR'). The four products were used as inputs to compute the shortwave irradiance by using the solar radiation (SRAD) model of Wilson and Gallant (2000), as described next. The reader is referred to Gutiérrez-Jurado and Vivoni (2012) for a description of the study site and products.

SRAD model

SRAD is a distributed model for complex terrain, which takes into account the interactions of solar radiation fluxes with atmospheric and land surface characteristics (Moore *et al*., 1991). Figure 1 presents a schematic of the SRAD model. The amount of solar irradiance reaching the ground at a location depends on a series of factors that operate over a range of scales (McKenney *et al*., 1999) spanning from global to microscale conditions. Global factors account for the solar beam angle of incidence and the distance travelled from the Sun to the Earth, which is dictated by latitude and time of the year. At the regional scale, several factors affect irradiance, including: (1) atmospheric attenuation (t) resulting from the

Copyright © 2012 John Wiley & Sons, Ltd.

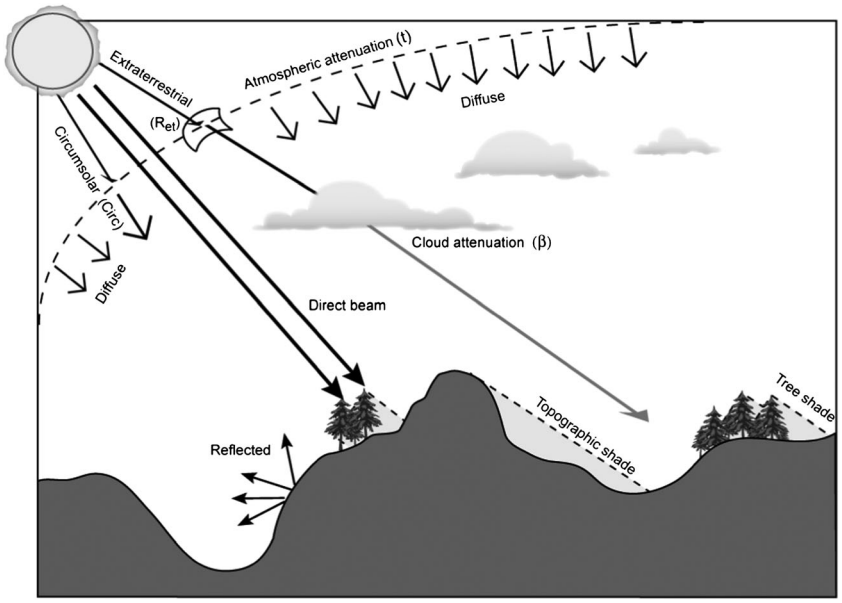

Figure 1. Schematic illustrating the incoming shortwave irradiance components and its attenuation: isotropic diffuse and circumsolar diffuse (*Circ*) irradiance, direct beam and reflected irradiance, atmospheric attenuation (t), cloud attenuation (β) and topographic and tree shading.

reflection, absorption and scattering of the solar beam by gases, water vapour and aerosols; (2) reemission of the absorbed and scattered irradiance in the atmosphere as isotropic diffuse radiation; (3) circumsolar radiation (*Circ*) emanating from within 5° of the solar disc; and (4) cloud attenuation (β) of the direct solar beam and diffuse irradiance. At the local scale, terrain conditions, such as slope and aspect, can alter the total irradiance (i.e. direct and diffuse) through reflection from the ground or through shading. Finally, tree canopies can reflect or absorb radiation, thus, controlling the amount of irradiance received by understory vegetation and intercanopy spaces (McKenney *et al*., 1999; Martens *et al*., 2000).

To compute the potential incoming shortwave radiation (SWR) for sloping terrain, SRAD requires calibrating the model to local site conditions (e.g. McKenney *et al*., 1999; Wilson and Gallant, 2000). Model calculations are performed on 12-min intervals and summed to daily fluxes for the majority of the direct, diffuse and reflected radiation fluxes (Figure 1). In order to obtain realistic values, SRAD requires mean monthly values of five radiation parameters that can be calculated using nearby data. In this work, incoming direct and diffuse shortwave radiation data were obtained from the Sevilleta Long Term Ecological Research (LTER) Red Tank weather station, located <1 km from the study basin. Table 1 presents the input variables and parameters necessary for SRAD. In the following, we provide a brief description of each input.

The circumsolar irradiance is the SWR originating 5° around the solar disc from which a coefficient (*Circ*) is derived to allow the calculation of the total incident irradiance. The coefficient *Circ* is calculated as (Wilson and Gallant, 2000):

$$Circ = \frac{R_{mth}}{24 \cdot I} \tag{1}$$

where R_{mth} is the mean daily observed irradiance for each month, averaged over a series of years, and I is the solar constant of 4.871 MJ m^{-2} h^{-1}.

Atmospheric transmittance (t) accounts for the attenuation of extraterrestrial irradiance and is calculated as the fraction of extraterrestrial irradiance observed at the ground on clear sky days minus a transmissivity lapse rate due to the thinning of the atmosphere with elevation, as:

$$t = \left(\frac{R_{et}}{R_{thcs}}\right) - 0.00008 \cdot z \tag{2}$$

where R_{et} is the extraterrestrial irradiance from the sun incident on a horizontal plane at the top of the atmosphere, 0.00008 is the transmissivity lapse rate and z is elevation above mean sea level (z is ~1700 m at the study site). R_{et} was calculated using the solar constant (I) and a series of geometric relations of the Sun distance and angles for each day of the year (Dingman, 2000).

Sunshine fraction (S) is the daily proportion of sunshine calculated by dividing the hours of clear sky insolation by the hours with cloudy conditions. This parameter is difficult to obtain as few weather stations directly report cloudiness on a consistent basis. As a result, monthly variations of S were obtained from the Albuquerque International Airport station located ~60 miles northeast of the study basin. The cloud transmittance coefficient (β) is a monthly fraction of attenuation of the direct and diffuse irradiance by clouds. β can be calculated as:

$$\beta = \left(\frac{R_{th}}{R_{thcs}} - S\right) \cdot (1 - S)^{-1} \tag{3}$$

where R_{th} and R_{thcs} are the mean monthly observed and clear sky irradiances, respectively; each averaged over several years. Clear sky irradiance is the flux of incoming

Copyright © 2012 John Wiley & Sons, Ltd.

Table I. Solar radiation calibration parameters.

Month	R_{th}* [MJ m^{-2}]	R_{mth}** [MJ m^{-2}]	R_{thcs}*** [MJ m^{-2}]	R_{et}† [MJ m^{-2}]	[R_{thcs}/R_{et}] [−]	$Circ$‡ [−]	Albedo [−]	b†† [−]	S*† [−]	t± [−]
January	390.1	12.8	14.2	18.7	0.76	0.11	0.2	0.62	70.1	0.62
February	449.5	16.2	19.3	23.7	0.82	0.14	0.2	0.67	69.1	0.68
March	673.3	21.7	25.0	30.1	0.83	0.19	0.2	0.64	73.3	0.70
April	779.9	26.0	30.1	36.0	0.83	0.22	0.2	0.68	80.1	0.70
May	887.7	29.0	33.3	39.9	0.83	0.25	0.2	0.68	80.1	0.70
June	886.1	29.4	34.3	41.5	0.83	0.25	0.2	0.70	83.9	0.69
July	841.4	27.1	33.2	40.7	0.82	0.23	0.15	0.68	77.1	0.68
August	758.1	24.5	30.1	37.5	0.80	0.21	0.15	0.67	75.1	0.67
September	656.5	21.9	25.9	32.4	0.80	0.19	0.17	0.69	78.5	0.66
October	561.9	17.9	21.2	26.0	0.81	0.15	0.2	0.67	78.0	0.68
November	413.9	13.9	16.8	20.2	0.83	0.12	0.2	0.67	73.9	0.69
December	364.1	11.6	13.5	17.3	0.78	0.10	0.2	0.62	69.6	0.64

*R_{th} is the total observed irradiance for a given month averaged over a series of years.
**R_{mth} is the mean daily observed irradiance for a given month averaged over a series of years.
***R_{thcs} is the mean monthly clear sky irradiance.
† R_{et} is the mean monthly extraterrestrial irradiance on a horizontal plane.
‡ $Circ$ is the mean monthly value for the circumsolar coefficient.
†† b is the monthly cloudy irradiance transmittance value.
*†S is the mean monthly sunshine fraction.
± t is the monthly value for atmospheric transmittance.

radiation when the sky is completely unobstructed by clouds or dust. The calculation of R_{thcs} is somewhat problematic when there is no cloud cover data associated directly to the radiation observations. We computed R_{thcs} following McKenney *et al*. (1999) by: (1) obtaining the maximum radiation values for each month for all years; (2) verifying that these maximum values correspond to the day of maximum insolation hours; (3) plotting the maximum daily irradiance for each month against the day of the year; (4) fitting a polynomial to the data from which clear sky radiation was calculated; and (5) obtaining the mean monthly clear sky irradiance (R_{thcs}) from the polynomial interpolation.

Albedo is the fraction of the incident radiation reflected by the land surface. This value can be measured in the field from SWR observations, or alternatively, values for albedo can be found in tables for different surfaces. In this study, the albedo was implemented uniformly across the basin with seasonal changes in the summer months because of vegetation greening. We explored the sensitivity of irradiance to changes in albedo because of differences in the land cover (north facing trees vs south facing shrubs) and their effects through increased or decreased reflection.

Comparison between simulated and observed irradiance

The performance of SRAD was verified by comparing mean monthly radiation estimates of 2 years against independent observations from a pyranometer located at the flat headslope of the basin. Figure 2 shows the comparison of the observed and simulated mean monthly radiation. Observed error bars represent ± 1 standard deviation of the temporal variation in each month, whereas the simulated error bars are ± 1 standard deviation of the spatial variations at pixels in close proximity to the measurement site. In general, the simulated irradiance agrees well with the observed radiation for winter, but differences between the two increase during summer months. These summer differences are likely due to poor sunshine fraction parameterization of the model. Note that sunshine fraction parameters were derived from available data at Albuquerque which may not capture local cloudiness given the small convective storm scale during the summer. Nevertheless, the SRAD estimates represent a potential maximum irradiance during the summer months and matches well with the clear sky radiation during this period, providing confidence in the simulated irradiance for the purposes of this study.

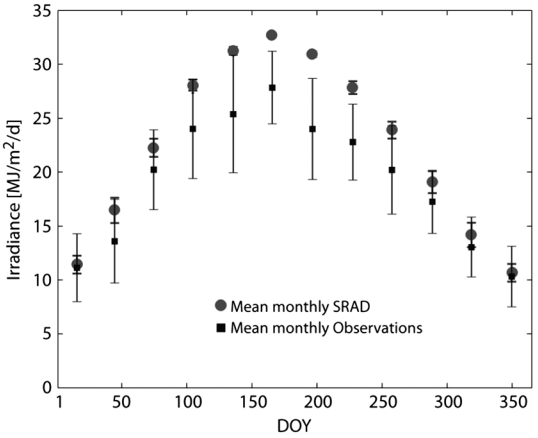

Figure 2. Comparison of mean monthly radiation estimates from pyranometer observations from study site (34.41°N, 106.97°W, 1706 m) and the solar radiation (SRAD) model. Error bars depict ± 1 standard deviation. The observed values were calculated over the period 2007–2008.

SOLAR RADIATION ANALYSES

Topographic and vegetation controls on annual irradiance

Annual irradiance estimates provide a first indication of the topographic controls in the opposing hillslope ecosystems. Figure 3 shows the spatial distributions of the total annual irradiance for each product: (a) IFSAR, (b) dGPS, (c) bare

Copyright © 2012 John Wiley & Sons, Ltd.

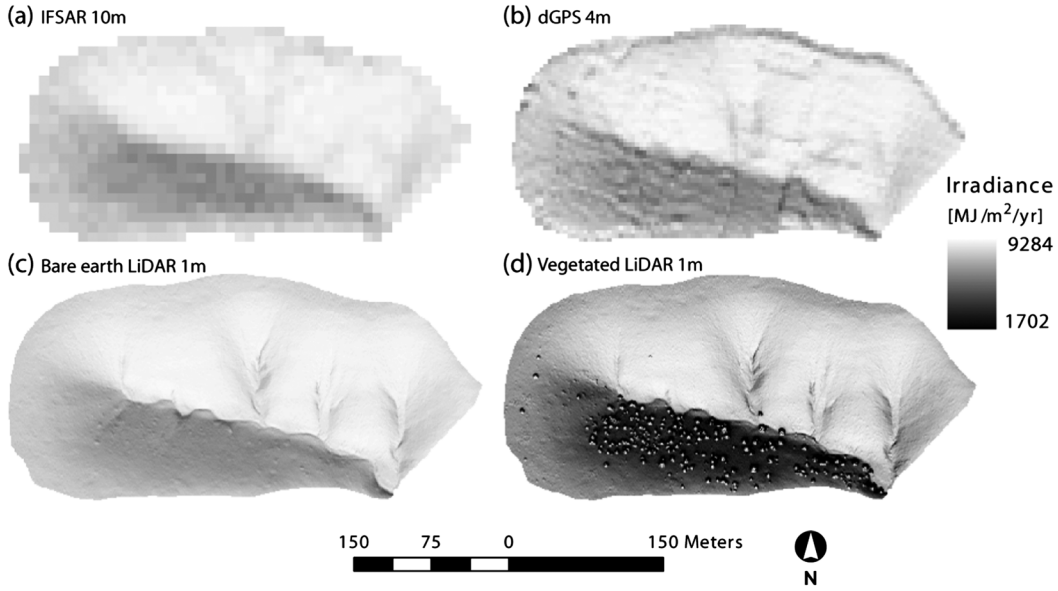

Figure 3. Spatial distributions of the total annual irradiance (MJ m^{-2} $year^{-1}$) for (a) IFSAR, (b) dGPS, (c) bare earth LiDAR and (d) vegetated LiDAR products.

earth LiDAR and (d) vegetated LiDAR. In all products, the contrast in total irradiance between the south and north facing slopes is evident. This contrast is even more pronounced for the vegetated LiDAR where annual differences between north facing and south facing slopes can reach 8000 MJ m^{-2} $year^{-1}$. This represents an 87% reduction in the irradiance for some north facing sites as compared to values on the south facing slope. In addition, there is a notable increase in the complexity of the irradiance field as fine scale topographic and vegetation details are included in the products. Also, note that the vegetated LiDAR indicates sharp contrasts between the shaded intercanopy areas and the exposed treetops. A common feature observed in all estimates is the influence of the slope in modifying the control of aspect on the irradiance. For example, the improved terrain definition in the LiDAR products indicates (1) low irradiance in very steep slopes (>25°) of north facing and west facing aspect and (2) high irradiance on steep to moderately steep slopes of south and southeast aspect.

To provide an assessment of the effects of aspect and slope, we plotted the mean annual irradiance for each major orientation [north (315–45°), east (45–135°), south (135–225°) and west (225–315°)] against slopes at 1° intervals in Figure 4. The general trends in this analysis include (1) irradiance for south facing areas increases non-linearly with steeper slopes, reaching a maximum at around 20°; (2) north facing and east facing areas show decreasing irradiance with increasing slope that is more marked and linear for north facing sites; and (3) west facing locations do not exhibit a strong irradiance trend with the slope. The impact of spatial resolution on annual irradiance is closely tied to the range of slope and aspect values in each product (see Gutiérrez-Jurado and Vivoni, 2012). In the study basin, this effect is more notorious for north facing locations. For instance, for each increase in resolution and quality (Figure 4a–c), there was an increase in the slope range (~7° for every product) and a corresponding ~1000 MJ m^{-2} $year^{-1}$ decrease in minimum irradiance. As a result, annual irradiance in north facing areas linearly decreases at a rate of ~140 MJ m^{-2} $year^{-1}$ per degree of slope for the IFSAR, dGPS and bare earth LiDAR products.

The effect of tree canopies on modulating the control of topographic slope and aspect on irradiance is particularly interesting. Note the rate of decrease in the irradiance on the north facing slope for the vegetated LiDAR (Figure 4d) is not monotonic as in the other products. Three regions are apparent: (a) Region I from 0 to 15° with a similar behaviour as the other products; (b) Region II from 15 to 25° with a steeper rate than in the other products (and than in Region I); and (c) Region III with slopes >25° that show no irradiance trend with the slope and exhibit very high variability. In addition, the irradiance values for the north facing slope have increasing dispersion (indicated by ± 1 standard deviation bars) with increasing slope. We interpret this variability to be a result of the complex effects of tree canopies on the north facing slope, including increasing their exposure on treetops and shading their surrounding intercanopy spaces. Although the shade and reflected irradiance produced by tree canopies should vary according to season, their impact is strong enough to alter the slope control on annual irradiance in north facing areas. These results agree well with Zou *et al.* (2007), who observed that the annual amount of near ground solar irradiance on north facing and south facing slopes is highly dependent on canopy cover.

Figure 5 presents the variation of annual irradiance across all aspects in each product. Bin-averaged annual irradiance, calculated for bin widths of 10° in aspect (denoted by the symbols), is similar among all products, although the variability in each aspect bin is different (dashed lines are ± 1 standard deviation). Coarse resolution DEMs (IFSAR and dGPS) have a more restricted range of aspect values and may miss entire east facing and west

Copyright © 2012 John Wiley & Sons, Ltd.

facing areas. Note that irradiance varies considerably within the north–northeast facing areas (larger spread) but is more uniform in the south facing regions, for all products. Clearly, north facing sites receive lower irradiance, with as

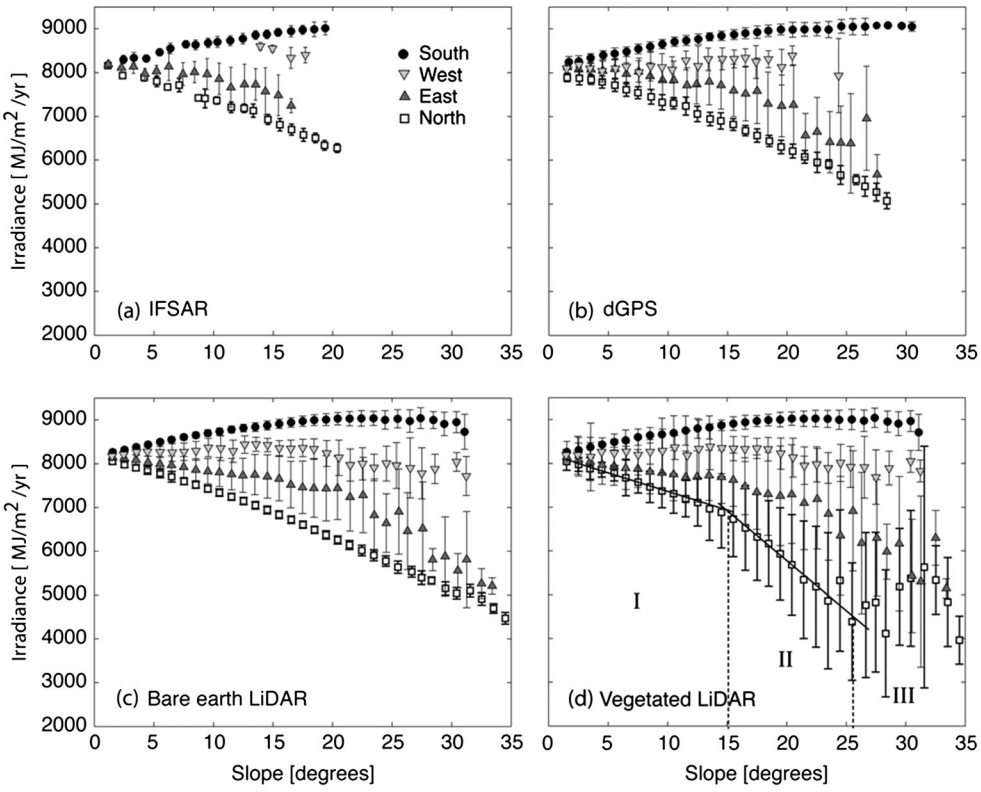

Figure 4. Total annual irradiance ($MJ\,m^{-2}\,year^{-1}$) for (a) IFSAR, (b) dGPS, (c) bare earth LiDAR and (d) vegetated LiDAR products as a function of slope and aspect.

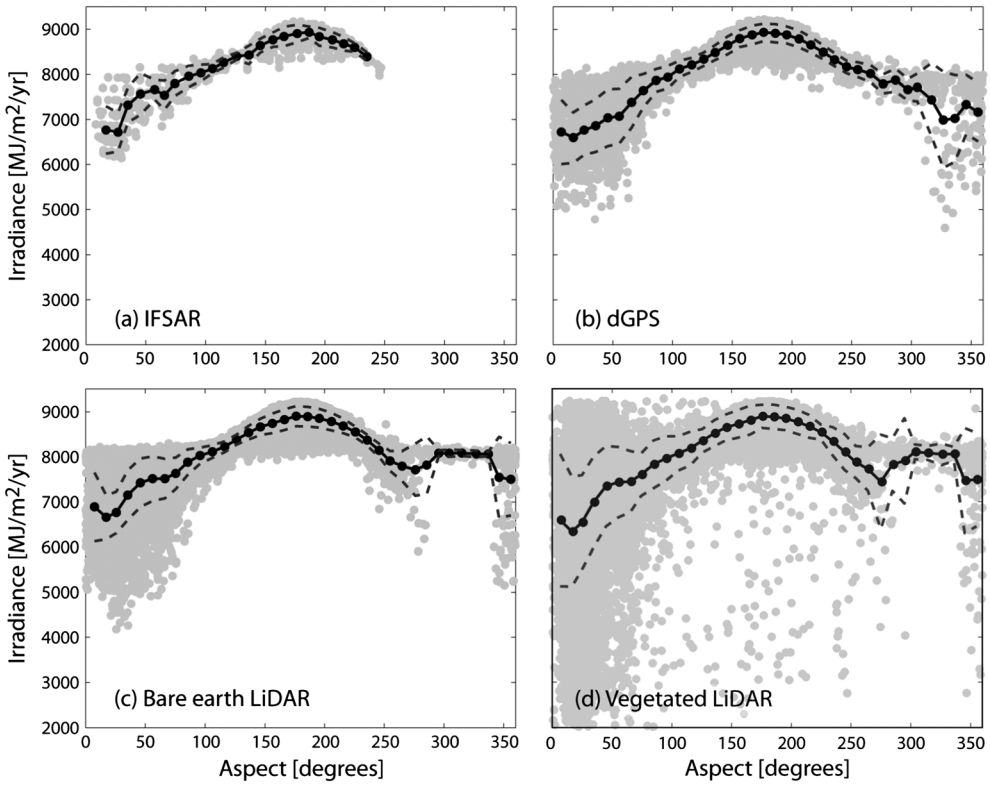

Figure 5. Total annual irradiance plotted as a function of aspect for each DEM: (a) IFSAR, (b) dGPS, (c) bare earth LiDAR and (d) vegetated LiDAR. The grey dots represent all the data; black circles show the mean irradiance for each aspect bin, and dashed lines are ± 1 standard deviation.

Copyright © 2012 John Wiley & Sons, Ltd.

much as a 2000 MJ m^{-2} year^{-1} difference as compared to south facing areas. Differences between the bare earth and vegetated LiDAR are evident in the north–northeast facing region but are not reflected in the bin-averaged values. The individual sites lying outside the ± 1 standard deviation in the north–northeast facing region are particularly affected by tree shading and have reductions of irradiance as high as 5000 MJ m^{-2} year^{-1}. This suggests that vegetation–radiation interactions in north facing areas can be substantial at the annual scale and, thus, merit closer inspection.

Another method used to depict irradiance differences in the basin is via the use of probability density functions (PDFs) of the annual irradiance for north facing and south facing locations, as shown in Figure 6. Interestingly, the annual irradiance distribution for south facing locations is remarkably similar for all products, suggesting that coarser terrain products are adequate in regions with high radiation fluxes. Conversely, irradiance PDFs for north facing sites exhibit clear differences near 6500–7000 and 7500–8000 MJ m^{-2} year^{-1} among the products. For example, north facing PDFs of the LiDAR products show a strong bimodality, reflecting the slope distribution, as shown in Gutiérrez-Jurado and Vivoni (2012). This bimodality is muted in the dGPS product and nearly identical in the IFSAR DEM. The effect of tree canopies in the vegetated LiDAR (Figure 6c) is limited to north facing areas and results in an overall dispersion of irradiance, with higher and lower values near the tails of the distribution, and a decrease in the bimodality. This suggests that the tree canopies increase the spatial variability in the north facing irradiance. Lower irradiance values (<6000 MJ m^{-2} year^{-1}) are due to tree shading effects on intercanopy spaces, whereas the higher irradiances (>8000 MJ m^{-2} year^{-1}) result from the exposure of south facing treetops (Figure 3d).

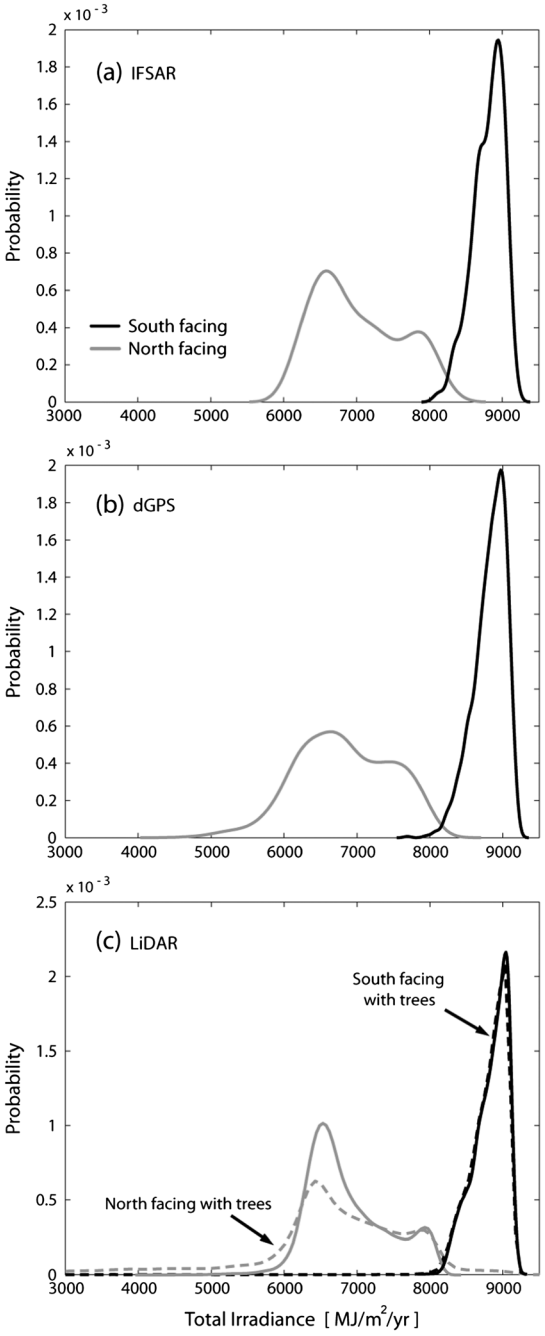

Figure 6. Probability density functions (PDFs) of the total annual irradiance for (a) IFSAR, (b) dGPS and (c) LiDAR products of south facing (black line) and north facing (grey line) slopes. Dashed lines in (c) illustrate the effects of tree shading and reflection.

Seasonal variability of topographic and vegetation controls

Because aspect-derived contrasts in irradiance are known to vary with the seasons (e.g. Walton *et al.*, 2005; Zou *et al.*, 2007), we assessed differences in daily irradiance in Figure 7 for the spring equinox (DOY 80), summer solstice (DOY 172) and winter solstice (DOY 355), where DOY is the day of year. In the northern hemisphere during the summer (winter) solstice, the Earth is tilted towards (away from) the Sun, leading to more (less) intense and longer (shorter) irradiance. During the spring equinox, the angle of the direct sun beam is intermediate, and irradiance values fall between the summer and winter solstices. Visually, the largest differences between north facing and south facing areas for the unvegetated DEMs (IFSAR, dGPS, bare earth LiDAR) occur during the winter solstice, and the smallest variations during the summer solstice. However, this contrast is not observed for the vegetated LiDAR, where the largest differences take place during the spring equinox. Note the dramatic impact of the trees during the various seasons, generally leading to lower irradiance in the north facing slope and increasing its spatial variability considerably. Although the increase in spatial resolution and accuracy improves seasonal irradiance estimates, the effect of the tree canopies overwhelms this improvement, leading to a more pronounced impact on the irradiance field. This suggests that tree height and cover information is essential in assessing microclimate conditions in semiarid basins with differences in vegetation patterns.

Figure 8 presents the combined effect of aspect and slope on the daily irradiance for three products (IFSAR, dGPS and vegetated LiDAR). We omit the bare earth LiDAR because the vegetated version best exhibits irradiance differences among the slopes. Clear aspect controls are observed for the spring equinox and winter solstice, increasing (decreasing) in irradiance with the slope

Copyright © 2012 John Wiley & Sons, Ltd.

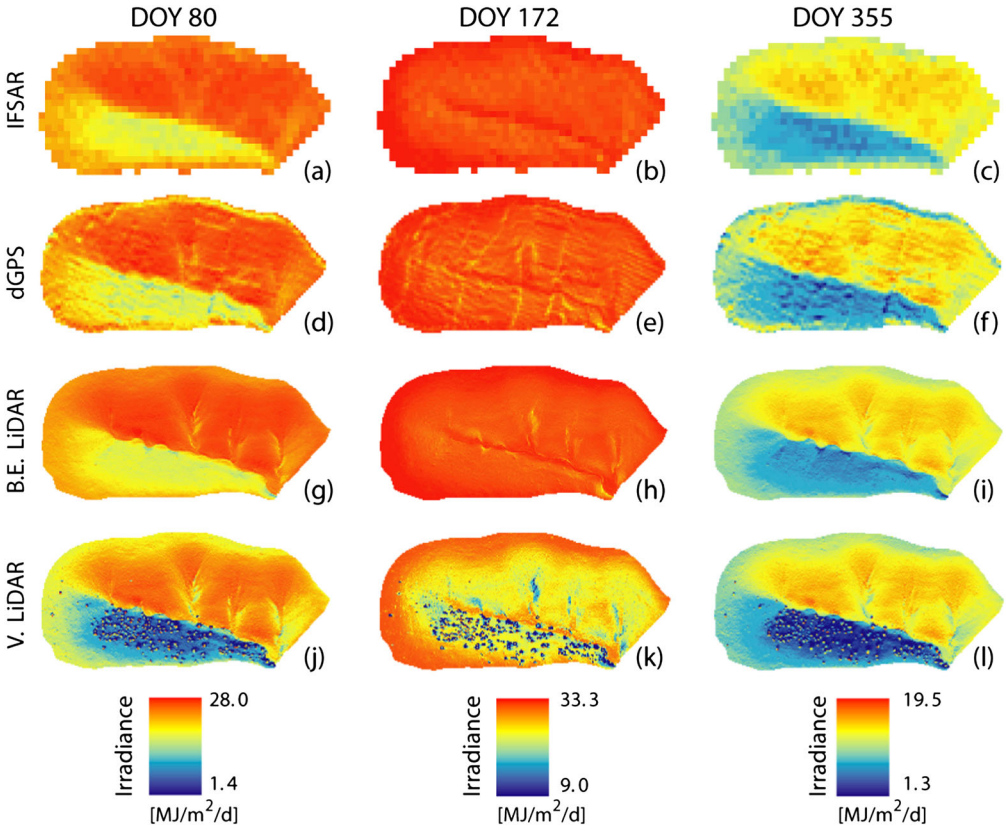

Figure 7. Spatial distributions of the daily irradiance for each DEM [top to bottom: (a-c) IFSAR, (d-f) dGPS, (g-i) bare earth LiDAR and (j-l) vegetated LiDAR], for the spring equinox (right column), summer solstice (middle column) and winter solstice (left column). Note that for each day of year (DOY), the four product maps were adjusted to the maximum range of values observed among the products for comparison purposes.

for the south facing (north facing) locations. These results closely parallel the annual irradiance dependence on slope and aspect but yield greater slope and aspect differences during the winter solstice. The controlling effects of aspect and slope on irradiance nearly disappear during the summer solstice in the IFSAR and dGPS DEMs and are greatly reduced in the vegetated LiDAR. Nevertheless, tree canopies influence the irradiance during the summer solstice, particularly for the steeper slopes, by reducing irradiance in the north facing and west facing locations (Figure 8h). The largest impact of the tree canopies occurs, however, during the spring equinox (Figure 8g), instead of the winter solstice. This is primarily due to the pronounced decrease in irradiance with the slope in north facing locations and suggests that the spring tree shading is more important at reducing the irradiance than in the winter time, when most of the shade is due to topographic effects. This has important ecological implications as the spring irradiance is closely related to the first pulse of grass productivity in intercanopy areas (Pennington and Collins, 2007; Ivanov *et al*. 2008b). Clearly, the availability of unvegetated and vegetated terrain products allows distinguishing tree versus topographic (slope and aspect) controls on the seasonal irradiance in the study basin.

Vegetation–irradiance interactions as a function of tree cover and albedo

An important question is the potential of vegetation feedbacks to the local radiation field as a function of tree cover (Breshears *et al*., 1998; Gutiérrez-Jurado *et al*., 2006). We explore this by inspecting mean irradiance differences (MID) during the year in two sampling areas (SA) with distinct tree cover percentages: (1) SA1 with 28% tree cover and (2) SA2 with 12% tree cover. Figure 9a shows the two SA in the north facing slope selected for this analysis. We evaluate the effect of tree radiation sheltering by subtracting the bare earth LiDAR radiation from the vegetated LiDAR radiation for each day in the year and for each SA as:

$$\mathrm{MID} = R_{veg} - R_{bare} \tag{4}$$

where R_{veg} and R_{bare} are the irradiances averaged over all intercanopy spaces in each SA after masking out the tree cells determined using an algorithm by Forzieri *et al*. (2009). Figure 9b shows the MID calculated for each day of the year for the two SA. A negative MID indicates that the SA experiences a reduction in radiation because tree shading overwhelms any potential increases in the reflection to the ground because of the tree albedo. For this analysis, the albedo values in Table 1 were assumed. In both SA, the trees reduce the amount of irradiance throughout the year, leading to a net loss of radiation that is greater during the summer season than the winter. The sampling area with higher tree cover (SA1) receives consistently less irradiance during the year, with SA1 and SA2 losing ~310 and ~220 $\mathrm{MJ\,m^{-2}\,year^{-1}}$, respectively. This implies that a 16% increase in the canopy cover from

Copyright © 2012 John Wiley & Sons, Ltd.

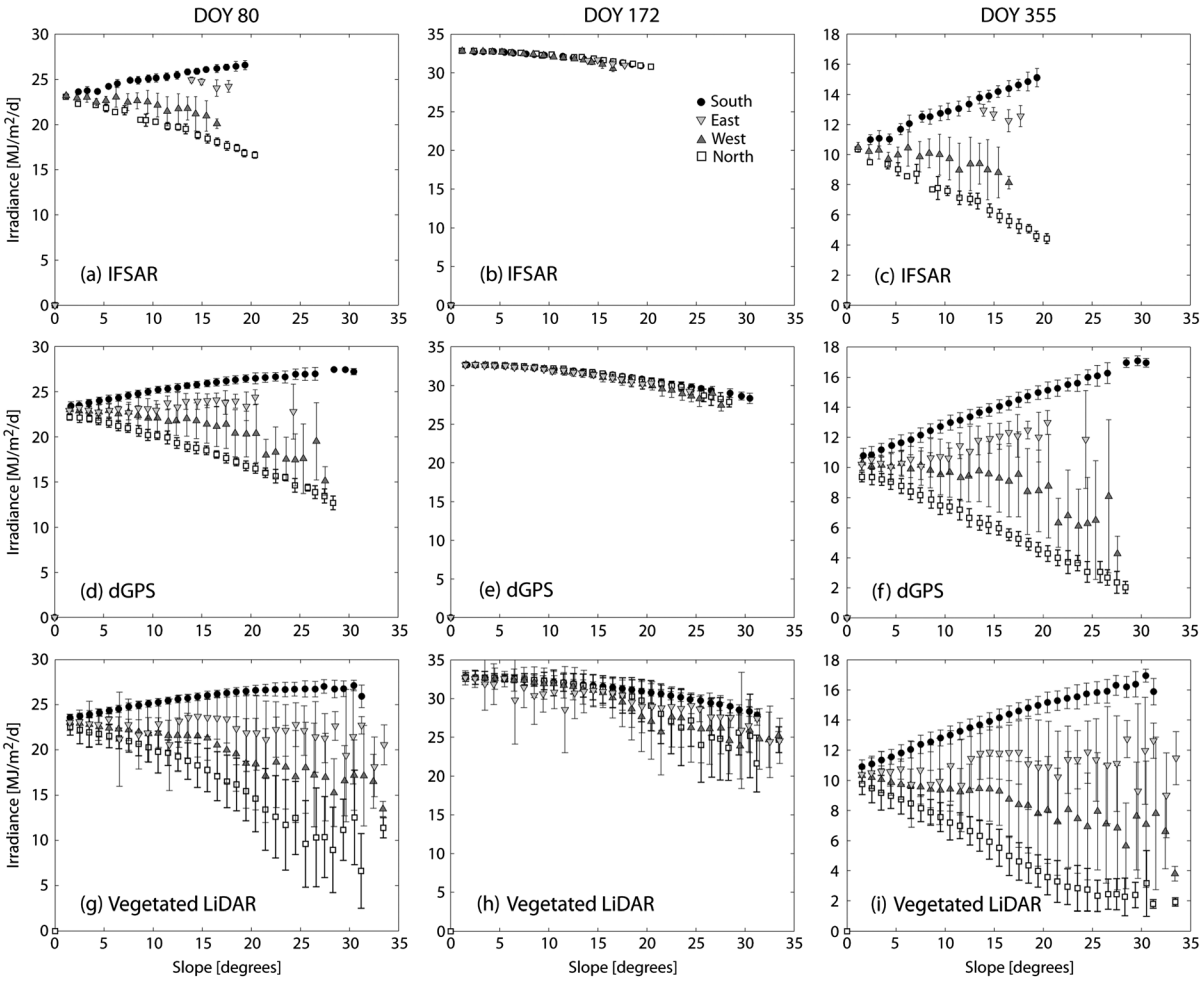

Figure 8. Daily irradiance as a function of slope for each DEM product [top to bottom: (a–c) IFSAR, (d–f) dGPS and (g–i) vegetated LiDAR], for spring equinox (right column), summer solstice (middle column), and winter solstice (left column). Irradiance values are grouped by aspect with different symbols.

SA2 to SA1 leads to a 40% decrease in annual irradiance. These results indicate that the trees affect the total amount of irradiance received by intercanopy spaces, depending on the tree cover and the day of the year. Overall, the denser tree cover in SA1 was more efficient in reducing the irradiance as compared to the sparser SA2 area.

To evaluate the combined effects of terrain attributes and tree cover, we subtracted the mean irradiance from the two SA for each product (vegetated and bare earth LiDAR) as:

$$\mathrm{MID}_{\mathrm{veg,bare}} = R(\mathrm{SA1})_{\mathrm{v,b}} - R(\mathrm{SA2})_{\mathrm{v,b}} \qquad (5)$$

where R(SA1) and R(SA2) represent the areally averaged irradiance for the intercanopy areas in each SA, and v and b depict the vegetated and bare earth products (note that $\mathrm{MID}_{\mathrm{veg}}$ is related to $R(\mathrm{SA1})_{\mathrm{v}}$ and $R(\mathrm{SA2})_{\mathrm{v}}$ only, similarly for $\mathrm{MID}_{\mathrm{bare}}$). $\mathrm{MID}_{\mathrm{veg}}$ and $\mathrm{MID}_{\mathrm{bare}}$ are the solid and dotted lines in Figure 9c, respectively. Temporal differences between $\mathrm{MID}_{\mathrm{veg}}$ and $\mathrm{MID}_{\mathrm{bare}}$ (depicted as the area between the solid and dotted lines) capture explicitly the role played by tree canopies on the irradiance, independent of variations in topographic conditions among the two SA. Note that the combined effects of changes in topographic conditions among the two SA and a 16% increase in tree cover from SA1 to SA2 produce a net loss of radiation of ~300 MJ m^{-2} year^{-1} ($\mathrm{MID}_{\mathrm{veg}}$). By removing the effect of the trees ($\mathrm{MID}_{\mathrm{bare}}$), a net annual irradiance loss of ~220 MJ m^{-2} year^{-1} is observed, which is a 26.6% increase in irradiance as compared to the $\mathrm{MID}_{\mathrm{veg}}$. It is interesting to note that the temporal variations in $\mathrm{MID}_{\mathrm{veg}}$ and $\mathrm{MID}_{\mathrm{bare}}$ reveal that the effect of the tree canopies on the irradiance is greatest during the summer period. Furthermore, the effect of topographic shading is largest during spring and fall seasons, suggesting that the impacts of terrain attributes and vegetation cover on irradiance are asynchronous during the year.

The impact of tree reflection was further assessed by performing a sensitivity analysis of the surface albedo. Prior results assumed a spatially uniform albedo with temporal fluctuations during the summer season (Table 1). For this analysis, a spatially variable albedo was used on the basis of vegetation differences (trees vs grasses/shrubs). Tree albedo was held constant at a value of 0.15 because of its evergreen nature, whereas the grass and shrub albedos were varied according to seasonal phenology (Table 1). Figure 10a and b illustrates the impact of the spatially variable albedo (dotted lines) with respect to the uniform albedo (solid lines). Results indicate a slight decrease in

Copyright © 2012 John Wiley & Sons, Ltd.

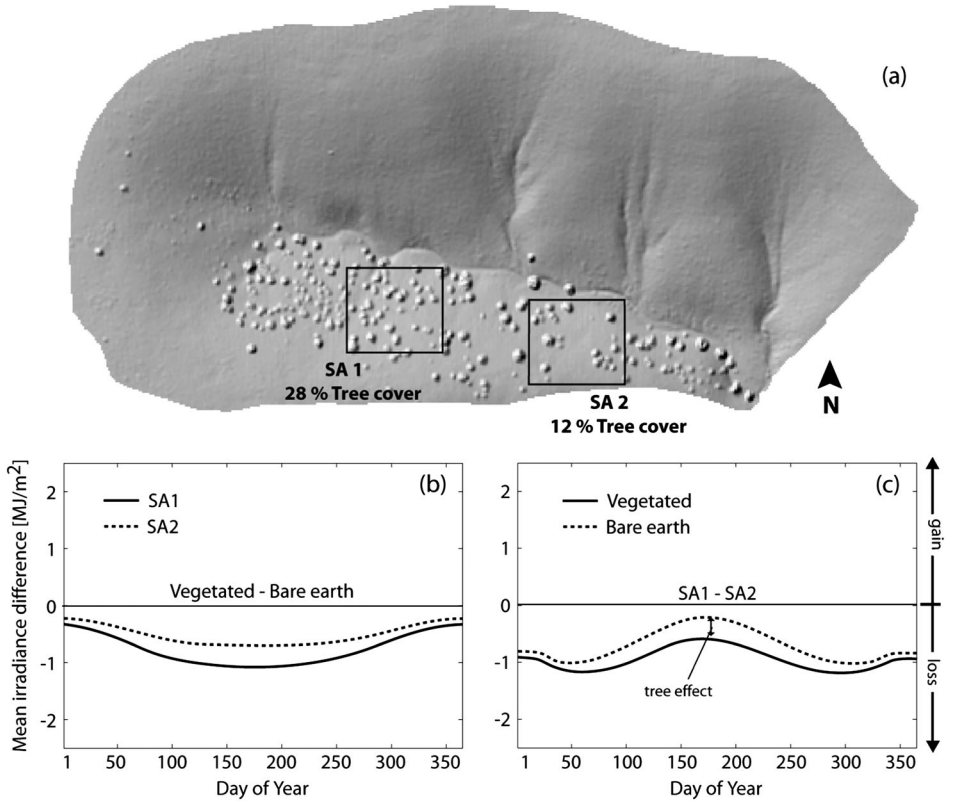

Figure 9. (a) Digital surface model depicting two sampling areas (SA) with different tree cover percentages: SA1 = 28% and SA2 = 12%; (b) mean irradiance difference between vegetated and bare earth sample areas; and (c) mean irradiance difference between SA1 and SA2 for vegetated (solid line) and bare earth LiDAR (dotted line).

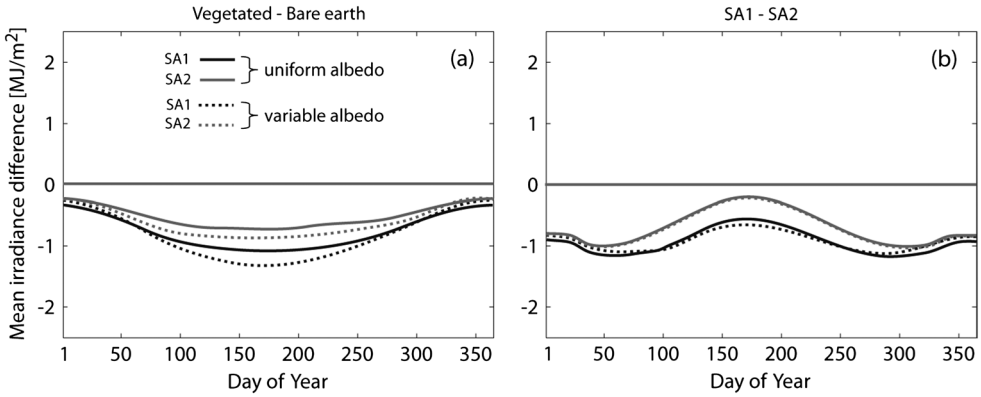

Figure 10. Sensitivity analyses for a spatially uniform albedo (solid lines) and a variable albedo (dotted lines). (a) Mean irradiance difference between vegetated and bare earth sample areas and (b) mean irradiance difference between SA1 and SA2 for vegetated (solid line) and bare earth LiDAR (dotted line).

irradiance when using a spatially variable albedo for both SA1 and SA2, especially during the summer (Figure 10a), but indicate a small irradiance gain in SA1 during winter. The decrease in irradiance in the summer is due to the lower albedo of trees (reduced from ~0.2 to 0.15), resulting in less radiation reflected back to the intercanopy spaces. The small increase in the winter for SA1 is likely due to the higher cover, suggesting slightly higher tree reflection to the intercanopy space at this tree density for this sun beam angle. The impact of the albedo on the tree effect (i.e. the difference between MID_{veg} and MID_{bare}, Figure 10b) is minimal but exhibits the trends described for summer and winter seasons. This suggests that using a spatially variable albedo amplifies the observed differences in radiation in the opposing slopes.

Individual tree locations and canopy radiation

Despite their close proximity, the hillslope ecosystems show irradiance differences at seasonal and annual scales. As a result, tree locations within the study basin should be controlled by aspect and, to a lesser extent, by slope. Figure 11a graphically shows the tree locations, with respect to aspect and slope in polar coordinates, with the distance from the origin representing the surface slope (0 to 40°). The majority of the trees are clustered in the north–northeast region

Copyright © 2012 John Wiley & Sons, Ltd.

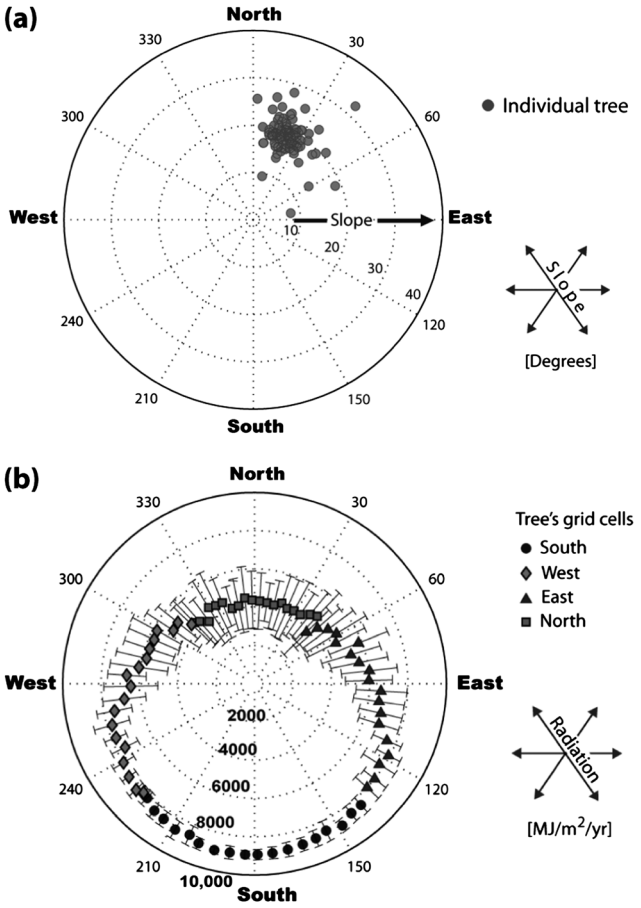

Figure 11. (a) Location of each individual tree as a function of aspect and slope and (b) Bin-averaged total annual irradiance for each tree aspect, separated into south (circles), west (diamonds), east (triangles) and north facing (squares) sites. Error bars depict ± 1 standard deviation in each bin. The magnitude of irradiance [MJ m^{-2} $year^{-1}$] increases radially outwards.

between 0 and 50° in aspect and along slopes between 15 and 25°. This suggests a preferential location (or topographic niche) for conifer trees related to the irradiance received at a site. This observation supports the analysis of Ivanov *et al.* (2008b) which indicated that grass species in this climate had preferential locations depending on radiation amounts. The range of slopes with trees also coincides with Region II in Figure 4d, indicating that the steepening of the irradiance trend with the slope in the north facing areas is due to tree sheltering.

Tree canopies at specific locations constitute a protuberance in the terrain with defined canopy aspects and slopes. Figure 11b shows the mean annual irradiance received by tree canopies in the basin as a function of aspect. Distance from the origin indicates the amount of irradiance on the trees themselves for each aspect bin (10° bin width). In general, the portions of the canopies facing north receive the least radiation (~4000 MJ m^{-2} $year^{-1}$), and the parts facing south receive the highest irradiance (~9000 MJ m^{-2} $year^{-1}$). Similarly, the spatial variability (±1 standard deviation within each aspect bin as bars) is greater for north facing sides, and it decreases when approaching the south facing parts. As a result, we would expect that intercanopy areas on the north facing slope, looking directly towards the south facing sides of a tree canopy, experience higher amounts of canopy reflectance. This effect can combine with lower shading in certain intercanopy areas of the north facing hillslope to result in a net increase of radiation throughout the year. This behaviour would contradict the general trend of decreased irradiance in the north facing hillslope and is only likely to occur under very special circumstances. For example, this may explain the small increase in irradiance in SA1 (higher tree density) during the winter season (Figure 10a).

Finally, we used the vegetated LiDAR to explore the relation of tree canopy height with three terrrain attributes: aspect, slope and curvature. We used tree height, extracted using an algorithm by Forzieri *et al.* (2009), to classify canopies into three sizes: small (<1 m), medium (1 to 2.5 m) and tall (>2.5 m). For each category, we calculated the probability of tree occurrence as a function of aspect, slope and curvature in Figure 12. Clearly, there are no differences in the tree height distribution with aspect as trees are located on north–northeast slopes. Nevertheless, the range of aspect values in which trees occur slightly increases with tree height. Slope appears to have an effect on the distribution of tree height with smaller trees (<1 m) located in a more restricted range of slopes (15 to 21°) as compared to medium-size trees (13 to 26°) and tall trees (5 to 30°). Note that small and medium trees have normal

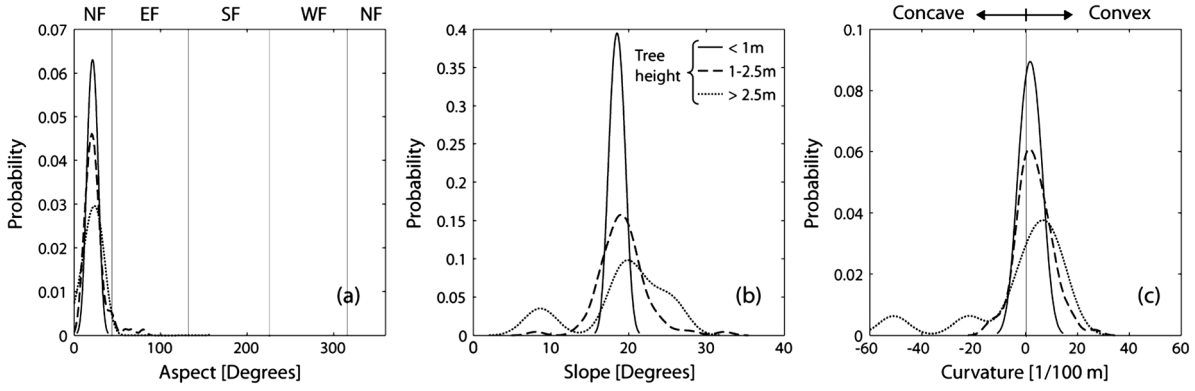

Figure 12. Probability density functions (PDFs) of tree height and location with respect to (a) aspect, (b) slope and (c) curvature. The solid line is for trees with heights of 1 m or less, the dashed lines is for trees between 1 and 2.5 m height, and the dotted line is for trees taller than 2.5 m. In (c), negative curvatures indicate concave terrain, whereas positive values indicate convex terrain.

Copyright © 2012 John Wiley & Sons, Ltd.

distributions of tree occurrence with slope, whereas tall trees exhibit a bimodal distribution such that they are located either on gently sloping terrain (5 to 12°) or steeper slopes (15 to 30°), with the majority located around 20°. With respect to curvature, we find that (1) the majority of small-size and medium-size trees are found on planar terrain and have almost equal chances of finding a tree on convex and concave locations, and (2) a few tall trees are located in concave areas (negative curvature), where soil water tends to concentrate, whereas the rest are found in more convex locations (positive curvature), associated with a diverging hillslope (Gutiérrez-Jurado and Vivoni, 2012). Although we would expect that tall trees be found in concave areas with water accumulation, this may not occur for all tall trees if they grow to a size that depends less on the local conditions of the terrain (concave or convex) by reaching out farther with a larger root system. Further exploration of this topic is warranted through the use of high-resolution topography–vegetation datasets.

CONCLUSIONS

Opposing hillslope ecosystems in mid-latitude, semiarid regions exhibit clear differences in vegetation composition and hydrogeomorphic properties. These differences are driven by variations in the energy budget in which solar irradiance plays an important role. Quantifying irradiance contrasts between the north facing and south facing hillslopes is a first approximation to unravelling the complex interactions leading to the observed ecogeomorphic patterns. In this work, we used a distributed solar radiation model and a set of sequentially improved elevation datasets to explore the vegetation–topography–radiation interactions at a basin in the Sevilleta National Wildlife Refuge. Previous studies addressing the effects of slope and aspect on annual irradiance found that polar-facing (equator) areas with steeper slopes receive less (more) radiation (Rich *et al*., 1995; Breshears *et al*., 1998; Zou *et al*., 2007). Our analysis on the effects of topography on irradiance supports prior studies and demonstrates that the slope–aspect effect on irradiance in the study basin is more prominent for the north facing areas, leading to a linear decrease rate of ~140 $MJ\,m^{-2}\,year^{-1}$ per degree increment of slope. In addition, the pronounced effect of the slope on north facing areas is augmented when the effect of the tree canopies is considered, leading to large reductions in total annual irradiance because of tree sheltering. Our analyses indicate that conifer trees effectively reduce annual and seasonal irradiance with important influences on their local microclimate in ways that can self-reinforce their occupation of the north facing slope. For example, we would expect that lower energy loads on the north facing slope would lead to lower evapotranspiration rates for intercanopy grasses, allowing higher soil moisture fluxes in the soil profile that sustain the deeper-rooted conifer trees (Gutiérrez-Jurado *et al*., 2006).

Assessing the performance of the various products on irradiance allowed us to elucidate the impact of spatial resolution on the vegetation–topography–radiation interactions at the basin scale. In general, improving the definition of terrain features (i.e. aspect, slope and curvature) by increasing the spatial resolution and quality leads to the amplification of the irradiance contrasts in the basin. However, annual irradiance estimates for south facing areas are remarkably similar for all products, suggesting that coarser terrain products are adequate in regions with high radiation fluxes. On the other hand, radiation fluxes on north facing locations are significantly improved with each increase in resolution (i.e. IFSAR to dGPS, dGPS to LiDAR). Moreover, adding the tree effects as obstructions in the irradiance estimates results in an increase of the spatial variability of radiation on the north facing hillslope and a significantly lower irradiance in the intercanopy spaces occupied by grasses. As a result, high-resolution data with tree cover information is essential in properly assessing microclimatic conditions in semiarid basins with opposing slopes. The varying energy loads between the mesic, north facing slope (juniper–grass ecosystem) and the more xeric, south facing slope (desert shrubland) support the hypothesis that the ecosystem patterns are primarily a result of the influence of aspect-controlled irradiance on local microclimate and its effects on water and energy fluxes on each hillslope (Gutiérrez-Jurado and Vivoni, 2012), whereas the terrain slope and the tree arrangements play secondary roles.

Seasonality in irradiance for water-limited ecosystems in areas of complex terrain is important in explaining the vegetation contrasts between opposing slopes (Dymond and Johnson, 2002; Badano *et al*., 2005; Walton *et al*., 2005). The fundamental premise is that the amount of radiation incident on the slopes varies through the seasons, providing more or less energy input for evapotranspiration demands (Breshears *et al*., 1998). For a basin in the northern hemisphere, we would expect to observe greater differences in irradiance between the north facing and south facing slopes in the winter and smaller differences during the summer. This behaviour in seasonal irradiance occurs in all products except the vegetated LiDAR product, where the largest irradiance differences between north facing and south facing slopes are found in the spring. The deviation from the expected results shows the impact of tree canopies in reducing the irradiance of their surrounding intercanopy areas. Given the grass community established between the conifer trees (Gutiérrez-Jurado *et al*., 2007), this finding has important implications on the radiation and thermal regime experienced during the spring growing season for the grasses (Pennington and Collins, 2007; Ivanov *et al*., 2008b). For instance, the cooler conditions and lower radiation created by tree shading may help conserve soil moisture in the intercanopy areas of the north facing slope through reduced evapotranspiration. In addition, the lower temperature and higher soil moisture created by differences in irradiance from tree shading could promote greater vertical fluxes in the soil profile that can sustain the deeper-rooted conifer trees.

The conifer trees (*J. monosperma*) are the only plant species fully captured by the LiDAR dataset in our study

Copyright © 2012 John Wiley & Sons, Ltd.

basin. Thus, the modelling of irradiance with tree canopy effects allowed us to examine in detail the potential feedback of conifers on irradiance. For two selected SA with varying tree cover percentage, we found that irradiance in intercanopy areas is reduced depending on the density of tree cover and the time of the year. We limited our analysis to the actual tree distribution on the north facing slope of the study basin. However, further investigation on the effect of spatial distribution of the canopies in adjacent basins of the region (Yetemen *et al*., 2010) may be required to clarify vegetation–radiation interactions in a broader setting, experiencing a wider variety of slope and aspects (Martens *et al*., 2000). Another issue regarding the effect of the trees on irradiance would be the proportion of radiation reflected from the different aspects of the canopy surface. For example, we observed that, on average, a conifer tree can receive twice as much radiation on the canopy surface facing south as compared to the canopy areas facing north. This explains why we observed greater variability in irradiance on the north facing slope of the vegetated LiDAR product.

An analysis of the spatial distribution of trees in relation to three topographic attributes (aspect, slope, curvature) showed that (1) tree locations are restricted to north facing areas and are normally distributed within the north–northeast region regardless of size, (2) small trees occur at restricted ranges of slopes (15–21°), whereas taller trees can be located either on steep or gentle slopes, and (3) the majority of the trees are located on slightly convex locations, whereas a few tall trees take advantage of the concave locations where water can accumulate in the landscape. The analysis of the spatial occurrence of conifer trees, with respect to terrain attributes, merits further investigation through a larger dataset (sample size) in the study region. Given the larger range of terrain and vegetation conditions in the broader region (Istanbulluoglu *et al*., 2008), this analysis is more likely to obtain generalized trends between tree establishment and terrain properties in this aspect-controlled ecosystem. In particular, a fruitful avenue for investigation is to link this observational dataset with numerical ecohydrological modelling (Ivanov *et al*., 2008a,2008b) in order to identify the underlying mechanisms (for example, lateral soil moisture redistribution through run-on or subsurface transport) that are responsible for the observed vegetation patterns.

ACKNOWLEDGEMENTS

We acknowledge research funding from the NASA Land Cover and Land Use Program (NNG05GA17G) and the NSF Geomorphology and Land Cover Dynamics Program (EAR-0819924). The NSF-sponsored National Center for Airborne Laser Mapping (NCALM) provided LiDAR data acquisition through their Seed Proposals for Graduate Students. The Sevilleta Long Term Ecological Research (LTER) and National Wildlife Refuge provided access to existing datasets and the research site. We also thank J. Bruce Harrison, Erkan Istanbulluoglu, Fred M. Phillips, Carlos F. Ramírez and Rafael L. Bras for discussions.

REFERENCES

Astrom M, Dynesius M, Hylander K, Nilsson C. 2007. Slope aspect modifies community responses to clear-cutting in boreal forests. *Ecology* **88**(3): 749–758.

Badano EI, Caviares LA, Molina-Montenegro MA, Quiroz CL. 2005. Slope aspect influences plant association patterns in the Mediterranean. *Journal of Arid Environments* **62**: 93–108.

Bennie J, Huntley B, Wiltshire A, Hill MO, Baxter R. 2008a. Slope, aspect and climate: spatially explicit and implicit models of topographic microclimate in chalk grassland. *Ecological Modelling* **216**: 47–59.

Bennie J, Hill MO, Baxter R, Huntley B. 2008b. Influence of slope and aspect on long-term vegetation change in British chalk grasslands. *Journal of Ecology* **94**: 355–368.

Breshears DD, Rich PM, Barnes F, Campbell K. 1997. Overstory-imposed heterogeneity in solar radiation and soil moisture in a semiarid woodland. *Ecological Applications* **7**(4): 1201–1215.

Breshears DD, Rich PM, Barnes FJ, Campbell K. 1998. Effects of woody plants on microclimate in a semiarid woodland: soil temperature and evaporation in canopy and intercanopy patches. *International Journal of Plant Sciences* **159**: 1010–1017.

Burnett BN, Meyer GA, McFadden LD. 2008. Aspect-related microclimatic influences on slope forms and processes, northeastern Arizona. *Journal of Geophysical Research* **113**: F03002. DOI: 10.1029/2007JF000789.

Caylor KK, Manfreda S, Rodriguez-Iturbe I. 2005. On the coupled geomorphological and ecohydrological organization of river basins. *Advances in Water Resources* **28**: 69–86.

Coblentz DD, Riitters KH. 2004. Topographic controls on the regional-scale biodiversity of the south-western USA. *Journal of Biogeography* **31**: 1125–1138.

Deng Y, Wilson JP, Bauers BO. 2007. DEM resolution dependencies of terrain attributes across a landscape, *International Journal of Geographical Information Science* **21**: 187–213.

Dingman LS. 2000. Physical Hydrology, 2nd edn. Prentice Hall: Upple Saddle River, New Jersey, USA.; 365.

Dymond CC, Johnson EA. 2002. Mapping vegetation spatial patterns from modeled water, temperature and solar radiation gradients. *Journal of Photogrammetry & Remote Sensing* **57**: 69–85.

Forzieri G, Guarnirei L, Vivoni ER, Castelli F, Preti F. 2009. Multiple attribute decision making for individual tree detection using high-resolution laser scanning. *Forest Ecology and Management* **258**: 2501–2510.

Fu P, Rich PM. 2002. A geometric solar radiation model with applications in agriculture and forestry. *Computers and Electronics in Agriculture* **37**: 25–35.

Guisan A, Zimmermann NE. 2000. Predictive distribution models in ecology. *Ecological Modelling* **135**: 147–186.

Gutiérrez-Jurado HA, Vivoni ER, Harrison JBJ, Guan H. 2006. Ecohydrology of root zone water fluxes and soil development in complex semiarid rangelands. *Hydrological Processes* **20**: 3289–3316.

Gutiérrez-Jurado HA, Vivoni ER, Istanbulluoglu E, Bras RL. 2007. Ecohydrological response to a geomorphically significant flood event in a semiarid catchment with contrasting ecosystems. *Geophysical Research Letters* **34**: L24S25. DOI: 10.1029/2007GL030994.

Gutiérrez-Jurado HA, Vivoni ER. 2012. Ecogeomorphic expressions of an aspect-controlled semiarid basin: I. Topographic analyses with high-resolution data sets. *Ecohydrology* **6**(1): 8–23.

Holland PG, Steyn DG. 1975. Vegetational responses to latitudinal variations in slope angle and aspect. *Journal of Biogeography* **2**: 179–183.

Holland PG, Steyn DG, Fuggle RF. 1977. Habitat occupation by *Aloe ferox Mill*. (*Liliaceae*) in relation to topographic variations in direct beam solar radiation income. *Journal of Biogeography* **4**(1): 61–72.

Horsch B. 2003. Modelling the spatial distribution of montane and subalpine forests in the Central Alps using digital elevation models. *Ecological Modelling* **168**: 267–282.

Ivanov VY, Bras RL, Vivoni ER. 2008a. Vegetation-hydrology dynamics in complex terrain of semiarid areas. I. A mechanistic approach to modeling dynamic feedbacks. *Water Resources Research* **44**: W03429. DOI: 10.1029/2006WR005588.

Ivanov VY, Bras RL, Vivoni ER. 2008b. Vegetation-hydrology dynamics in complex terrain of semiarid areas: 2. Energy-water controls of

Copyright © 2012 John Wiley & Sons, Ltd.

vegetation spatiotemporal dynamics and topographic niches of favorability. *Water Resources Research* **44**: W03430. DOI: 10.1029/2006WR005595.

Istanbulluoglu E, Yetemen O, Vivoni ER, Gutiérrez-Jurado HA, Bras RL. 2008. On the topographic imprint of vegetation: inferences from regional analysis of landscape morphology in central New Mexico. *Geophysical Research Letters* **34**: L14403. DOI: 10.1029/2008GL034477.

Kienzle S. 2004. The effect of DEM raster resolution on first order, second order and compound terrain derivatives. *Transactions in GIS* **8**: 83–111.

Kirkpatrick JB, Nunez M. 1980. Vegetation–radiation relationships in mountainous terrain: eucalypt dominated vegetation in the Risdon Hills, Tasmania. *Journal of Biogeography* **7**: 197–208.

Lassueur T, Joost S, Randin CF. 2006. Very high resolution digital elevation models: do they improve models of plant species distribution? *Ecological Modelling* **198**: 139–153.

Martens SN, Breshears DD, Meyer CW. 2000. Spatial distributions of understory light along the grassland forest continuum: effects of cover, height, and spatial pattern of tree canopies. *Ecological Modelling* **126**: 79–93.

Meentemeyer RK, Moody A, Franklin J. 2001. Landscape-scale patterns of shrub-species abundance in California Chaparral: the role of topographically mediated resource gradients. *Plant Ecology* **156**: 19–41.

McKenney DW, Mackey BG, Zavitz BL. 1999. Calibration and sensitivity analysis of a spatially-distributed solar radiation model. *International Journal of Geographical Information Science* **13**: 49–65.

Montero G, Escobar JM, Rodriguez E, Montenegro R. 2009. Solar radiation and shadow modelling with adaptive triangular meshes. *Solar Energy* **83**: 998–1012.

Moore ID, Grayson RB, Ladson AR. 1991. Digital terrain modelling: a review of hydrological, geomorphological, and biological applications. *Hydrological Processes* **5**: 3–30.

Nieve M, Abrahams AD. 2002. Vegetation influences on water yields from grassland and shrubland ecosystems in the Chihuahuan Desert. *Earth Surface Processes and Landforms* **27**: 1011–1020.

Paola C, Foufoula-Georgiou E, Dietrich WE, Hondzo M, Mohrig D, Parker G, Power ME, Rodriguez-Iturbe I, Voller V, Wilcock P. 2006. Toward a unified science of the Earth's surface: opportunities for synthesis among hydrology, geomorphology, geochemistry, and ecology. *Water Resources Research* **42**: W03S10. DOI: 10.1029/2005WR004336.

Pennington DD, Collins SC. 2007. Response of an aridland ecosystem to interannual climate variability and prolonged drought. *Landscape Ecology* **22**(6): 897–910.

Piedallu C, Gégout J. 2008. Efficient assessment of topographic solar radiation to improve plant distribution models. *Agricultural and Forest Meteorology* **148**: 1696–1706.

Ranzi R, Rosso R. 1995. Distributed estimation of incoming direct solar radiation over a drainage basin. *Journal of Hydrology* **166**: 461–478.

Rich PM, Hetrick WA, Savings SC. 1995. Modelling topographical influences on solar radiation: manual for the SOLARFLUX model. LA-12989-M, Los Alamos National Laboratories: Los Alamos; 33.

Rinehart AJ, Vivoni ER, Brooks PD. 2008. Effects of vegetation, albedo and solar radiation sheltering on the distribution of snow in the Valles Caldera, New Mexico. *Ecohydrology* **1**: 253–270.

Slatton KC, Carter WE, Shrestha RL, Dietrich W. 2007. Airborne laser swath mapping: achieving the resolution and accuracy required for geosurficial research. *Geophysical Research Letters* **34**: L23S10. DOI: 10.1029/2007GL031939.

Suri M, Hofierka J. 2004. A new GIS-based solar radiation model and its application to photovoltaic assessments. *Transactions in GIS* **8**(2): 175–190.

Tarolli P, Arrowsmith JR, Vivoni ER. 2009. Understanding earth surface processes from remotely sensed digital terrain models. *Geomorphology* **113**: 1–3.

Walton JC, Martinez-Gonzalez F, Worthington R. 2005. Desert vegetation and timing of solar radiation. *Journal of Arid Environments* **60**: 697–707.

Wilcox BP, Breshears DD, Allen CD. 2003. Ecohydrology of a resource conserving semiarid woodland: effects of scale and disturbance. *Ecological Monographs* **73**: 223–239.

Wilkinson MT, Humphreys GS. 2006. Slope aspect, slope length and slope inclination controls of shallow soils vegetated by sclerophyllous heath – links to long-term landscape evolution. *Geomorphology* **76**: 347–362.

Wilson JP, Gallant JC. 2000. Terrain Analysis: Principles and Applications. John Wiley & Sons: New York, New York, USA; 469.

Yetemen O, Istanbulluoglu E, Vivoni ER. 2010. The implications of geology, soils, and vegetation on landscape morphology: Inferences from semiarid basins with complex vegetation patterns in central New Mexico, USA. *Geomorphology* **116**: 246–263.

Zaksek K, Podobnikar T, Ostir K. 2005. Solar radiation modelling. *Computers & Geosciences* **31**: 233–240.

Zhang W, Montgomery DR. 1994. Digital elevation model grid size, landscape representation, and hydrologic simulations. *Water Resources Research* **30**: 1019–1028.

Zou CB, Barron-Gafford GA, Breshears DD. 2007. Effects of topography and woody plant canopy cover on near-ground solar radiation: relevant energy inputs for ecohydrology and hydropedology. *Geophysical Research Letters* **34**: L24S21. DOI: 10.1029/2007GL031484.

Copyright © 2012 John Wiley & Sons, Ltd.